Variability of Cloud Vertical Structure during ASTEX Observed from a Combination of Rawinsonde, Radar, Ceilometer, and Satellite

JUNHONG WANG

Program in Atmospheric and Oceanic Sciences, University of Colorado, Boulder, Colorado

WILLIAM B. ROSSOW

NASA/Goddard Institute for Space Studies, New York, New York

TANEIL UTTAL

NOAA/ERL/Environmental Technology Laboratory, Boulder, Colorado

MARGARET ROZENDAAL

Department of Earth and Environmental Sciences, Columbia University, New York, New York

(Manuscript received 22 May 1998, in final form 14 November 1998)

ABSTRACT

The macroscale cloud vertical structure (CVS), including cloud-base and -top heights and layer thickness, and characteristics of multilayered clouds, is studied at Porto Santo Island during the Atlantic Stratocumulus Transition Experiment (ASTEX) by using rawinsonde, radar, ceilometer, and satellite data. The comparisons of CVS parameters obtained from four different approaches show that 1) by using the method developed by Wang and Rossow rawinsonde observations (raob's) can sample all low clouds and determine their boundaries accurately, but oversample low clouds by about 10%, mistaking clear moist layers for clouds; 2) cloud-base heights less than 200 m in the radar data are ambiguous, but can be replaced by the values measured by ceilometer; and 3) the practical limit on the accuracy of marine boundary layer cloud-top heights retrieved from satellites appears to be about 150–300 m mainly due to errors in specifying the atmospheric temperature and humidity in the inversion layer above the cloud. The vertical distribution of clouds at Porto Santo during ASTEX is dominated by low clouds below 3 km, a cloud-free layer between 3 and 4 km, and ~20% high clouds with a peak occurrence around 7–8 km. Low clouds have mean base and top heights of 1.0 km and 1.4 km, respectively, and occur as single layers 90% of the time. For double-layered low clouds, the tops of the uppermost layers and the bases of the lowermost layers have similar distributions as those of single-layered clouds. The temporal variations of low clouds during ASTEX are apparently dominated by advecting mesoscale (20–200 km) horizontal variations. Coherent time variations are predominately synoptic (timescale 4.5–6.8 days) and diurnal variability. On the diurnal timescale, all cloud properties show maxima in the early morning (around 0530 LST) decreasing to minima in the late afternoon. Diurnal variations appear to be altered when high clouds are present above low clouds. The general characteristics of CVS in three ASTEX and the First ISCCP Regional Experiment (FIRE87) regions derived from a 20-yr rawinsonde dataset are also presented. The results suggest that CVS characteristics obtained from data collected at Porto Santo during ASTEX (June 1992) are not representative of other marine stratiform cloud regions.

1. Introduction

Marine stratocumulus clouds undergo considerable diurnal and synoptic variations in their horizontal and vertical structure (e.g., Short and Wallace 1980; Minnis and Harrison 1984; Betts 1990; Blaskovic et al. 1991; Klein and Hartmann 1993; Albrecht et al. 1995; Randall et al. 1996). Two stratocumulus regimes have been studied extensively in recent field experiments. One is characterized by horizontally uniform cloudiness, day and night, but with elevated cloud bases and thinner cloud layers during the daytime (Betts 1990; Blaskovic et al. 1991). This regime was studied during the First ISCCP (International Satellite Cloud Climatology Project) Regional Experiment (FIRE) near San Nicholas Island off the southern California coast in June–July 1987 (Albrecht et al. 1988; Randall et al. 1996). The other regime

Corresponding author address: Dr. Junhong Wang, NCAR/SSSF, P. O. Box 3000, Boulder, CO 80307-3000.
E-mail: junhong@ucar.edu

is characterized by a transition from horizontally extensive stratus and stratocumulus to cumulus under stratocumulus and then to broken, ''trade wind'' cumulus (Albrecht et al. 1995). This regime was studied during the Atlantic Stratocumulus Transition Experiment (ASTEX) between the Madeira and Canary Islands in June 1992. The former case is associated with a relatively shallow and well-mixed boundary layer, while the latter case has a much deeper boundary layer that is not always well mixed, exhibiting multilayer structure within the boundary layer. The differences in the vertical thermodynamic and turbulent structures of the marine boundary layer in these two cases are also revealed in their different cloud vertical structures (CVS), including the locations and variations of cloud base, cloud top, as well as cloud-layer thicknesses and the occurrence and characteristics of multilayered clouds. Hence measurements of CVS and its variations are analyzed to understand the behavior of the boundary layer (cf. Blaskovic et al. 1991; Albrecht et al. 1995; Randall et al. 1996; Miller et al. 1998).

Cloud boundaries can be measured by surface radars (e.g., Kropfli et al. 1995) and lidars (e.g., Sassen 1991), particularly when used together (Uttal et al. 1995). Several types of radar, lidar, and ceilometer have been successfully operated during a number of field experiments, such as ASTEX and FIRE. These datasets can provide useful information on CVS for various cloud types, but we have to understand their limitations. Radar, lidar, and ceilometer each have different limitations on sensitivity: longer-wavelength radars are less sensitive to the smaller cloud particles, lidar signals can be attenuated before reaching the top of moderately thick clouds, and ceilometers do not usually penetrate the lowest cloud layer to measure the boundaries of upper-level cloud layers (cf. Uttal et al. 1995). Therefore, a combination of these surface-based remote sensors is necessary to provide the most accurate and complete information about CVS. Still such surface-based remote sensors only provide ''pointlike'' measurements that do not sample the horizontal variations of the clouds. Moreover, the number of suitably equipped surface sites is small, leaving many cloud regimes unobserved and, until recently, these datasets rarely covered an extensive time period sufficient to examine variation statistics. Thus, the surface-based remote sensing observations need to be combined with other observations to obtain more complete sampling of cloud variations.

Measurements by imaging and sounding radiometers on weather satellites can be used to study the horizontal and vertical variations of cloudiness covering a much larger range of time- and space scales than surface-based or aircraft-based instruments; however, current satellite instruments can only observe the location of the uppermost cloud top, not the full vertical profile of cloud mass. Detailed satellite studies of marine boundary layer clouds were performed in relation to the FIRE87 (Minnis et al. 1992) and ASTEX experiments. The ISCCP global datasets can also be analyzed to examine the variations of boundary layer clouds (Randall et al. 1996; Rozendaal et al. 1995). The cloud variations observed in the global satellite results can be better interpreted by comparing them with the more detailed surface remote sensing results.

Since at least 1979, rawinsonde measurements of humidity profiles have been used to find cloud layers for synoptic forecasts (AWS 1979). Poore et al. (1995) combined such a rawinsonde analysis with surface cloud observations to provide a survey of cloud-layer thicknesses. Wang and Rossow (1995, hereafter WR95) developed an improved analysis method to determine CVS from rawinsonde observations (raob's). This method was validated by comparing cloud-top pressures with those obtained from satellites by ISCCP and cloud occurrence, low cloud-base heights, and overlap statistics with those reported in surface cloud observations. However, the evaluation in WR95 lacked comparison of cloud boundaries with independent measurements from surface-based remote sensors, so more quantitative assessments of this method's accuracy are desirable.

This paper has three goals. The first one is to compare different observation methods to evaluate each of them. The emphasis is on comparing the raob-determined CVS for low-level clouds with observations by radar and ceilometer during ASTEX. If the raob analysis can be validated, then the much larger observation record covering several decades at about 1000 stations around the globe can be used to extend the FIRE87 and ASTEX results to other types of boundary layer clouds and complement the extensive satellite results for cloud-top locations. The second goal is to combine all the observations to understand the sampling of each type of observation (i.e., what each is seeing), and to understand the characteristics and variability of marine boundary layer cloud vertical structure at Porto Santo during ASTEX. The third goal is to analyze the satellite data over the large area to investigate the interaction between spatial and temporal variations and analyze a 20-yr raob dataset in three ASTEX and the FIRE87 regions to provide information on typical CVS attributes in those regions.

ASTEX was conducted over the northeast Atlantic Ocean (Fig. 1) during June 1992 (Albrecht et al. 1995). An 8-mm (35 GHz) cloud-sensing Doppler radar, developed at the National Oceanic and Atmospheric Administration's Environmental Technology Laboratory (NOAA/ETL) (Intrieri et al. 1995), and the Colorado State University (CSU) laser ceilometer were operated at Porto Santo Island during ASTEX. Eight rawinsondes per day were launched from Porto Santo during the entire experiment. All datasets used in this study are described in section 2. Radar and ceilometer data are used to validate raob-derived cloud boundaries in section 3 and the satellite results in section 4. The combined analysis of the radar, ceilometer, rawinsonde, and satellite data provides information on the vertical distribution of cloud boundaries and their synoptic and di-

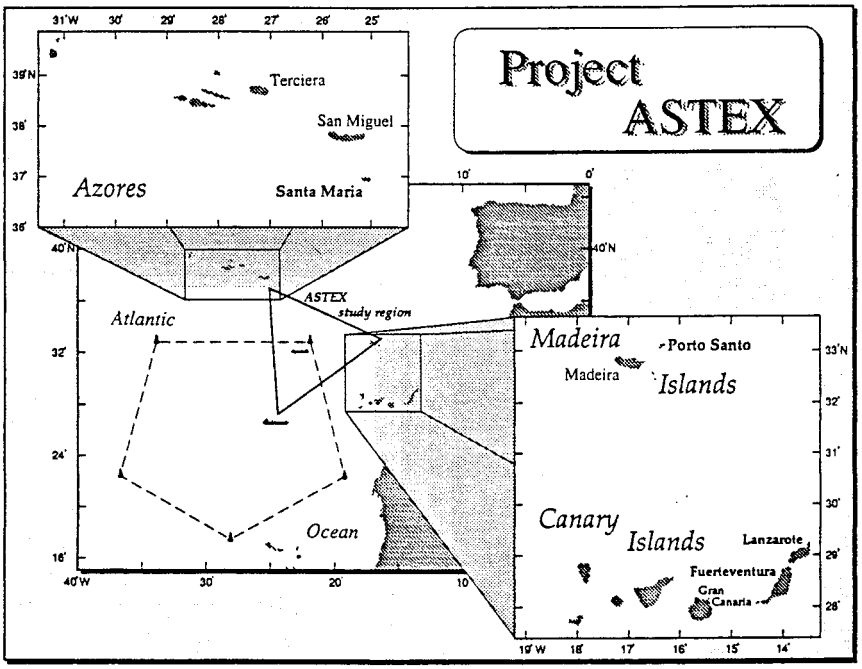

FIG. 1. ASTEX study region (adapted from Randall et al. 1996).

urnal variations at Porto Santo Island (section 5). We also examine the variety of results obtained at two other ASTEX locations and the FIRE87 region using a 20-yr global rawinsonde dataset. A summary is provided in section 6.

2. Data and analysis method

a. Rawinsonde data

During the entire ASTEX period, eight rawinsondes per day were launched from Porto Santo [33°5′2″N latitude, 16°20′49″W longitude, 97 m above mean sea level (MSL)] in the Madeira Island group (Fig. 1). A detailed explanation of the analysis of the rawinsonde dataset at Porto Santo is presented by Schubert et al. (1992). From 1 to 28 June 1992, 203 soundings were obtained. The raw rawinsonde data report temperature, humidity, and winds at irregular pressure and height levels, so they have been interpolated to uniform intervals with different vertical resolutions (5 s, 20 m, and 2 mb), preserving the highest possible vertical resolution (Schubert et al. 1992). We use the 20-m data in this study. In section 3, we apply the analysis described below to this rawinsonde dataset to obtain CVS information and compare CVS from rawinsonde data to that from radar–lidar and satellite data.

The general quality of the ASTEX raob's was quite good (Schubert et al. 1992). These data are superior to conventional raob's because of the much higher vertical resolution and more frequent time sampling (every 3 h). The higher vertical resolution overcomes the disadvantage of conventional raob's in detecting thin cloud layers, especially since typical marine stratocumulus clouds exhibit thicknesses of 100–300 m.

Another cloud boundary dataset is produced from all available operational raob's from the global upper-air observation network covering 20 years (1976–95) (Wang 1997). The dataset covers about 1000 stations around the globe; observations are available twice daily (0000 and 1200 UTC) from most of the stations. The mean vertical resolution of this dataset is 53 mb. In section 5c, the analysis method described below is applied to a subset of this global rawinsonde dataset to study CVS in three ASTEX and the FIRE87 regions and their differences. The subset dataset includes rawinsonde data at stations over three square regions (27°–34°N, 13°–19°W; 36°–40°N, 24°–32°W; 22°–33°N, 21°–35°W), representing three ASTEX regions (Madeira Islands, Azores Islands, and ocean; see Fig. 1), and at San Nicolas Island (33.3°N, 119.5°W) where FIRE87 took place. There are two operational World Meteorology Organization rawinsonde stations (32.63°N, 16.9°W and 28.47°N, 16.25°W) in the Madeira Island region, and one station (38.75°N, 27.07°W) in the Azores; the rawinsonde data in the ocean region consist of raob's from ships passing through this region.

b. Rawinsonde analysis to determine CVS

The analysis method used to determine CVS from rawinsonde humidity and temperature profiles is described in WR95. Cloudy layers are identified by high relative humidity (RH) values above a threshold value. Cloud-layer top and base are also identified by sudden

RH jumps that are positive at the base and negative at the top, respectively. The various forms in which humidity is reported (specific humidity, dewpoint temperature, dewpoint depression, or RH with respect to liquid water) are all converted to RH with respect to liquid water at temperatures ≥ 0°C and RH with respect to ice at temperatures < 0°C. The RH profile is then examined from the surface to the top to find cloud layers using a threshold RH value of 84% but also requiring that maximum RH exceed 87% within the cloud layer. In addition, RH is required to jump by at least 3% at cloud top and base. We call this method the standard method. For ''single level'' clouds, which have the same level identified as top and base, the cloud-layer top is assigned at half the distance to the next level above and the base is at half the distance to the next level below. Clouds were detected in 190 out of the total of 203 soundings at Porto Santo during ASTEX.

Some of the raob-detected low cloud layers might be clear but very humid layers, as discussed in WR95, since RH can exceed 87% near the surface without the formation of clouds, especially in the humid boundary layer over tropical and subtropical oceans. Direct comparison of coincident cloud layers reported by raob's using the standard method and radar implies that some raob-detected cloud layers, inside which RH $<90\%$ at all levels, do not have matched radar detections. Therefore, in this study we increased the two RH thresholds from 84% to 90% and 87% to 93%, respectively (referred as the ''90% alternate method''). All results presented below are produced by using this 90% alternate method, except where otherwise indicated. Using the alternate method the number of soundings containing clouds was reduced to 168.

c. Radar data

An 8-mm ETL cloud-sensing Doppler radar was operated at Porto Santo during ASTEX from 1 to 29 June 1992. Cloud boundaries are determined from radar time–height cross sections by using a data animation program called CLDSTATS, which is described by Uttal et al. (1993). The cloud boundary data are obtained in vertically pointing mode at 3-s intervals, reporting the base and top heights of each cloud layer at 3-s intervals for 24 min out of every 30 min. The results have a vertical resolution of 37.5 m and extend up to a height of 12 km. Since the radar can penetrate most clouds, there will be more than one cloud base–top pair when multiple cloud layers are present. There are total of 274 702 cloudy radar profiles and 343 432 cloud layers. Comparisons of the cloud boundary statistics from the 8-mm radar with those from a 3-mm radar and a 10.6-μm lidar during FIRE II demonstrate that the 8-mm radar can accurately sense very detailed cloud structures and is especially successful in detecting multiple cloud layers (Uttal et al. 1995).

The 8-mm radar has problems measuring cloud base heights <350 m because of ''ground clutter'' and power leakage problems. The ground clutter problem is due to the fact that the sidelobes of the radar antenna beam pattern receive energy reflected from the surface. The power leakage problem is a leakage of some transmitter power to the receiver when the receiver makes measurements very close in time to the pulse transmission time, that is, at very close ranges. Those effects preclude reliable detection of radar returns from any cloud bases within some finite height above the surface. To avoid these problems, we remove clouds with base heights <400 m and top heights <500 m in the radar data by reexamining the variations of cloud bases and tops with time. In this study, we use this new version of the radar data.

The 3-s temporal resolution of radar data is much higher than 3 h for rawinsonde data collected during ASTEX and satellite data. Because of high-frequency CVS variations discussed in section 5b, the difference in temporal resolution between radar and rawinsonde/satellite data needs to be taken into account. Therefore, we distinguish between results from the original 3-s radar data and from 3-h sampled radar data (data collected at times when rawinsonde and satellite have observations) when comparing radar-observed CVS with that from rawinsonde and satellite data in sections 3 and 4. In section 5, we only use 3-s radar data to calculate hourly mean values to preserve high-frequency variations. The version of data used is indicated explicitly in the following sections.

d. Ceilometer data

The CSU laser ceilometer was operated at Porto Santo Island during ASTEX to measure the base height of the lowest cloud layers up to 3480 m. The ceilometer data are available from 31 May to 28 June 1992 with a vertical resolution of 15 m and a temporal resolution of 1 min. Cloud fraction can also be estimated from ceilometer data by counting the number of 1-min reports with and without clouds (Bretherton et al. 1995). An hourly low cloud fraction dataset is formed.

e. Merged radar–ceilometer data

The radar's ground clutter and power leakage effects can cause uncertainties in radar-measured cloud-base heights below 350 m. The ceilometer data are used to verify the radar-determined lowest cloud-base heights. Figure 2 shows the lowest cloud-base heights detected by the radar, ceilometer, and raob's. There is good agreement between the radar and ceilometer for base heights above 600 m; both distributions exhibit peaks at 0.6–0.8 km and 1.6–1.8 km. However, the high frequency (34%) of cloud bases at 190 m in the radar data adjacent to 0% frequency at 300 m suggests false detections. In the reminder of this study of cloud boundaries, we replace the 190-m cloud-base heights in the radar data

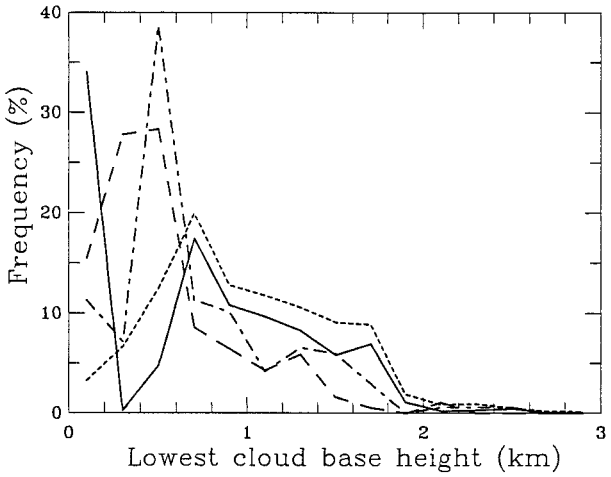

FIG. 2. Frequency distribution of base heights AGL of the lowest cloud layers below 3 km AGL during ASTEX from the radar data (solid line), the ceilometer data (the small dashed line), and the rawinsonde data using the standard method (long dashed line) and using the ''90% alternate method'' (dotted–dashed line).

with the time-matched ceilometer data to create a merged radar–ceilometer dataset. Those cloud layers without matched ceilometer data (46% of total) are considered false clouds and are discarded in the merged data. The merged data maintain the 3-s temporal resolution of radar data.

f. Satellite data

The satellite observations of cloud-top temperatures, pressures, and heights come from the new ISCCP analysis (Rossow et al. 1996). For the ASTEX region and time, the ISCCP D1 dataset is obtained from an analysis of infrared and visible radiances measured by the *Meteosat-4* geostationary weather satellite operated by the European Space Agency. Radiance calibration is determined by comparison with the ISCCP reference standard (see Brest et al. 1997). The image data are first sampled to intervals of 30 km and 3 h; the DX dataset reports the analysis results for individual image pixels and the D1 dataset summarizes these pixel-level results at a spatial resolution of 280 km. We make most extensive use of the results from the one D1 map grid cell that contains Porto Santo but also examine detailed variations using the DX dataset, including the single satellite pixel located nearest Porto Santo. The monthly mean cloud cover for this location is 68.5%, of which 54.2% are low-level clouds. Mean cloud optical thickness for low clouds is 5.4.

Cloud-top temperature is retrieved from the measured infrared (IR) radiance in the ISCCP analysis and converted into cloud-top pressures using the Television Infrared Observation Satellite (TIROS) Operational Vertical Sounder (TOVS) atmospheric temperature–pressure profiles. Monthly mean values are 278.9 K and 755 mb, respectively; for low-level clouds the mean values are 282.2 K and 809 mb, respectively. Cloud-top heights can then be calculated from these profiles using the hydrostatic equation, where the sea level is 1000 mb (the ''D1 method''). In an alternative method suggested by Minnis et al. (1992), cloud-top heights are calculated from the difference between surface and cloud-top temperatures by using a fixed temperature lapse rate value of 6.5 K km^{-1} (the ''D2 method''). Monthly mean values for all clouds and low-level clouds are 1.9 km and 1.4 km, respectively.

3. Comparison of rawinsonde-derived cloud boundaries with radar and ceilometer data

a. Comparison of cloud boundary statistics

The frequency distributions of cloud boundaries (top and base), layer thickness, and cloud occurrence as a function of height above ground level (AGL, all heights discussed in this section are heights AGL) from all available merged radar–ceilometer and raob's results are shown in Fig. 3 for all cloud layers from the surface up to 12 km. Both datasets show 1) the strong predominance of clouds below 2 km (59% and 74% for radar–ceilometer and raob's, respectively), 2) a cloud-free region between 3 and 4 km, and 3) a broad distribution of higher-level cloud occurrences between 6 and 10 km with a peak at 7–8 km. The raob's cloud-top height distribution agrees very well with that from the radar, particularly the two peaks at 1.2–1.4 km and 1.6–1.8 km. Both datasets show that most cloud layers are <1 km thick (83% and 87% for radar and raob's, respectively). For cloud-base heights, the radar–ceilometer data show a peak in the range 600–800 m, whereas the raob results show that 25% of the clouds have bases between 400 and 600 m.

Although ASTEX was designed to study marine boundary layer clouds, more than 20% of the clouds in this area occur above 4 km (consistent with ISCCP observations shown in Randall et al. 1996) and their effects on the boundary layer clouds should be studied. If the upper-level clouds overlie boundary layer clouds, then the ISCCP type of analysis will, under some circumstances, retrieve a cloud top at middle levels (cf. Baum and Wielicki 1994; Jin and Rossow 1997). The vertical distribution of top heights of the uppermost cloud layers from the ISCCP VIS/IR analysis is also shown in Fig. 3b: about 80% of the cloud tops are located below 3 km, but most of the cloud tops above that level are determined to lie between 3.5 and 9 km, suggesting an underestimate because of underlying clouds. This is consistent with the fact that 90% of all low-level clouds and 28% of all upper-level clouds occur alone, but 72% of upper-level clouds occur over a lower-level cloud and may be misplaced in the satellite analysis.

The frequencies of occurrence of one-, two-, and three-layered clouds from radar–ceilometer and raob da-

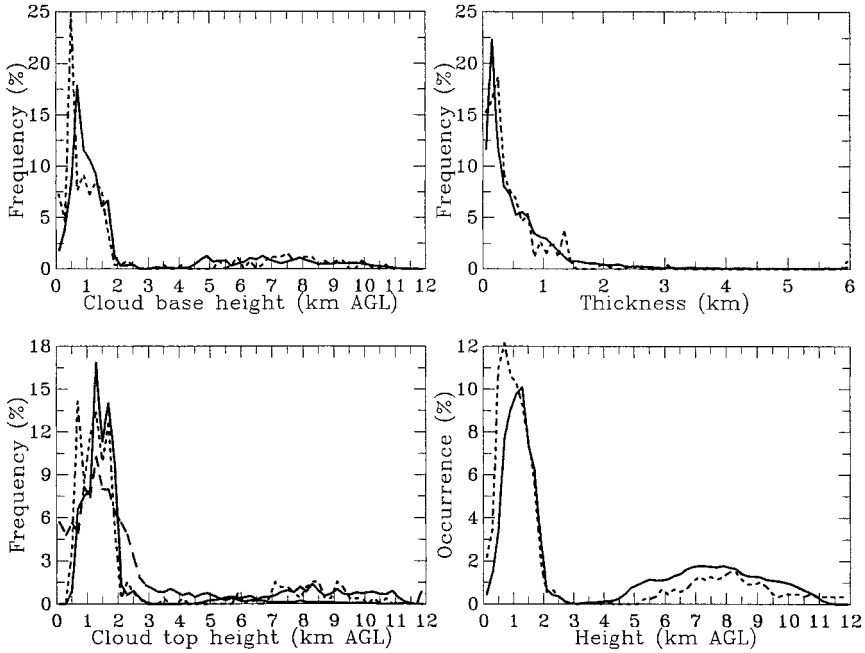

FIG. 3. Frequency distribution of cloud-base and -top heights AGL, layer thickness, and occurrences deduced from the merged radar–ceilometer data (solid line) and the rawinsonde data (dotted line) using the 90% alternate method at Porto Santo Island during ASTEX. The long dashed line for cloud-top height is from ISCCP VIS/IR analysis.

tasets are displayed in Fig. 4 for all cloud layers and only for cloud layers below 3 km. Including all cloud layers, raob's report less single-layered clouds but more two- and three-layered clouds than the radar: overall, there are 18% more multilayered clouds from raob's than from the radar. After excluding cloud layers above 3 km, multilayered clouds occur less frequently in both datasets, but raob's still detect 14% more multilayered clouds than the radar. Figure 5 shows the vertical distribution of clouds in two-layered systems when they are all below 3 km. The location of the uppermost cloud layer determined by the raob's corresponds very well with that from the radar–ceilometer, with frequency peaks at 1.3 km for the cloud base and two peaks at 1.3 and 1.7 km for the cloud top. For the lowermost cloud layer, the two datasets exhibit good agreement for the location of the cloud tops; the disagreement in cloud-base locations is similar to that shown in Fig. 3 for all cloud layers.

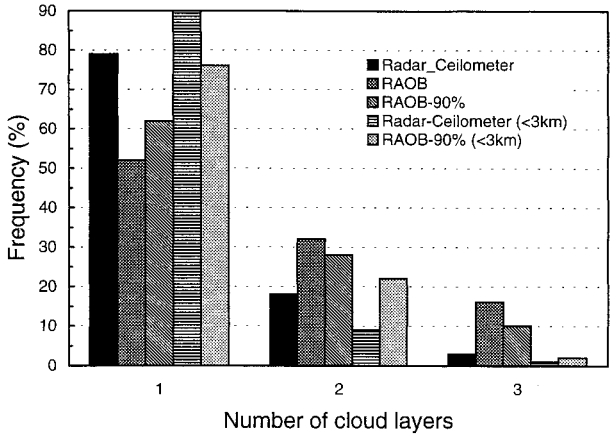

FIG. 4. The frequencies of one-, two-, three-, and more-than-three-layered clouds for all cloud layers in the radar–ceilometer data (Radar–Ceilometer), and the rawinsonde data using the standard analysis method (raob's) and using the 90% alternate method (raob–90%), and for cloud layers below 3 km AGL.

b. Explanations of disagreements between raob's and radar

As described in section 2b, we increased the RH thresholds by 6% from the standard values based on the fact that some of raob-detected low cloud layers appear to be clear but very humid layers. This produced several improvements in the comparison of CVS obtained from raob's and radar–ceilometer. First of all, there is better agreement in the frequencies of one-, two-, and three-layered clouds (Fig. 4). Second, the revised raob's capture the secondary peak of cloud-top heights at 1.3 km for the uppermost layer of two-layered systems, which is missed when using lower RH thresholds (Fig. 5). Third, raob's identify 17% more cases with the lowest cloud-base height in the range 0.4–1.8 km, in much better agreement with the ceilometer data (total frequency 88%); nevertheless, the raob cloud-base height distribution is still spread over the 0–0.6-km range in-

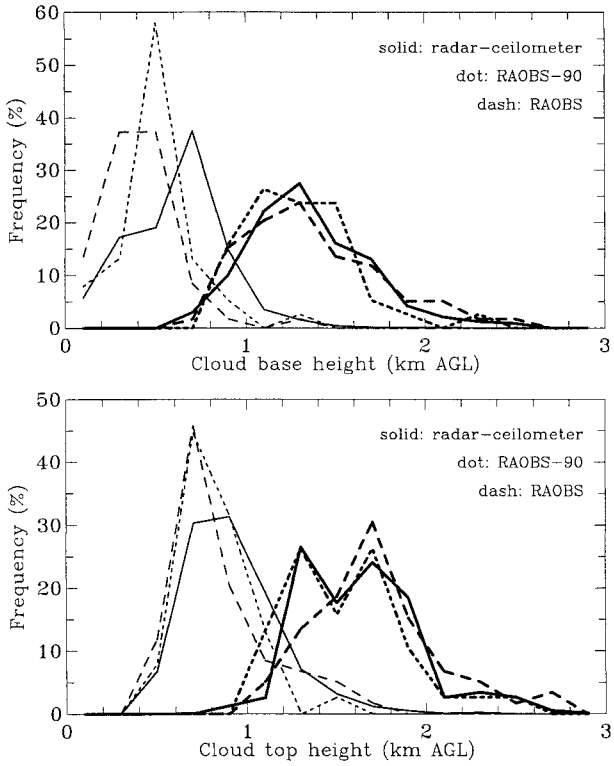

FIG. 5. Frequency distribution of (a) cloud-base and (b) -top heights AGL for two-layered low cloud system from radar–ceilometer data (solid), raob's with the 90% alternate method (dotted), and raob's with the standard method (dashed). The thin lines are for the lower layer and thick lines for higher layers.

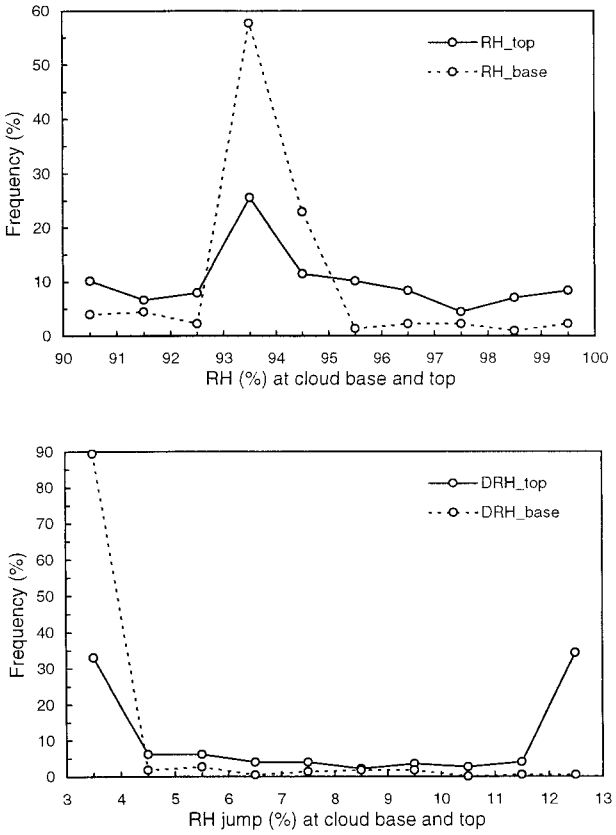

FIG. 6. Frequency distribution of RH (upper panel) and RH jump (lower panel) at raob-determined cloud base (solid line) and top (dotted line) using the 90% alternate method.

stead of being concentrated at 0.6–0.8 km as the ceilometer shows (Fig. 2).

The remaining question is why there is good agreement between raob's and radar cloud-top heights (Figs. 3 and 5), while the raob-determined cloud-base heights differ systematically from the ceilometer values even when the RH thresholds are increased (Fig. 2). Figure 6 shows the distribution of RH and RH jump (ΔRH) values at the cloud-base and -top locations determined using the 90% alternate method. Cloud-top locations are characterized by higher RH and ΔRH than cloud-base locations (note that the distribution peaks at RH = 93% and ΔRH = 3% in Fig. 6 result from the thresholds used in our analysis method). Thirty-eight percent of RH values are $\geq$95% and 41% of ΔRH values are $\geq$10% at cloud tops, compared with 9% and 1% at cloud bases, respectively. Figure 6 demonstrates that cloud tops are more distinct in the RH profiles (probably because of the capping inversion in the stratocumulus regime) and, therefore, insensitive to changes in the RH and ΔRH thresholds, whereas cloud base is sensitive as we have shown. This behavior makes it difficult to accurately estimate cloud bases using raob's, which is consistent with other studies (Albrecht et al. 1995). The 8-mm radar reflectivity profiles support this interpretation because they show that the reflectivity drops from its peak value to undetectable levels over an interval of 75 m at cloud top but shows smaller gradients near the lowest cloud bases (Albrecht et al. 1995).

Raob's were conducted every 3 h (0000, 0300, 0600, . . . , 2100 UTC) and only sample CVS at one instant at one particular time. However, the merged radar–ceilometer data have 3-s time resolution for 24 min out of every 30 min with the remaining 6 min for collecting data, and sample the temporal variations of CVS on timescales down to 3 s. Because of the lack of data for 6 min out every 30 min, the radar can be considered to have complete sampling of CVS on a half-hour timescale. When comparing CVS from raob's and radar, two factors have to be taken into account: 1) CVS variations on the timescale less than 3 h, that is, comparing raob's with all radar data within half-hour bins centered at 0000, 0300, . . . , 2100 UTC, and 2) the sampling noise, that is, comparing raob's with one radar sample randomly selected within half-hour bins around 0000, 0300, . . . , 2100 UTC. We found that the CVS properties calculated from all radar data within half-hour bins around 0000, 0300, . . . , 2100 UTC are essentially the same as that from all radar data with full 3-s resolution, implying small CVS variations on timescales between 0.5 and 3 h (Fig. 7). However, the sampling noise in-

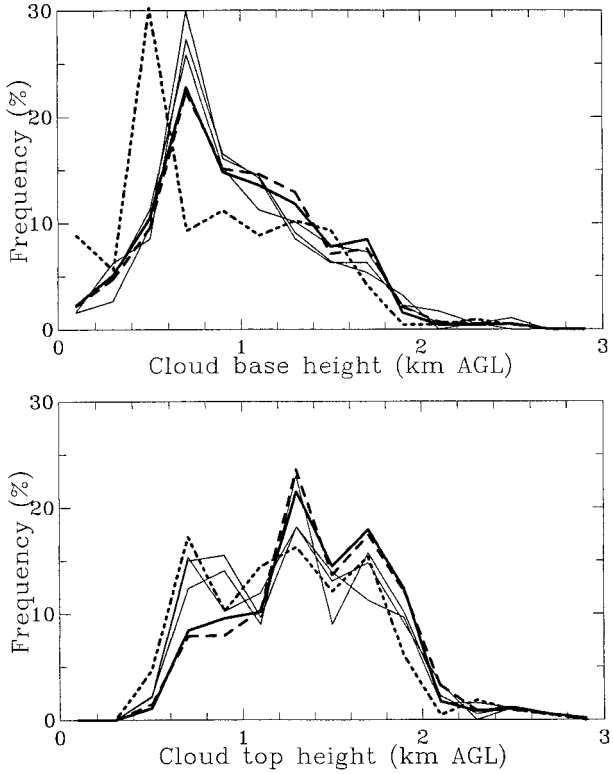

FIG. 7. Frequency distribution of low (a) cloud-base and (b) -top heights AGL from all 3-s radar–ceilometer data (thick solid); raob's with the 90% alternate method (thick dotted); all 3-s radar–ceilometer data within half-hour bin centered at 0000, 0300, . . . , 2100 UTC (thick dashed); and three 3-s radar–ceilometer samples randomly selected within half-hour bin centered at 0000, 0300, . . . , 2100 UTC (three thin solid lines).

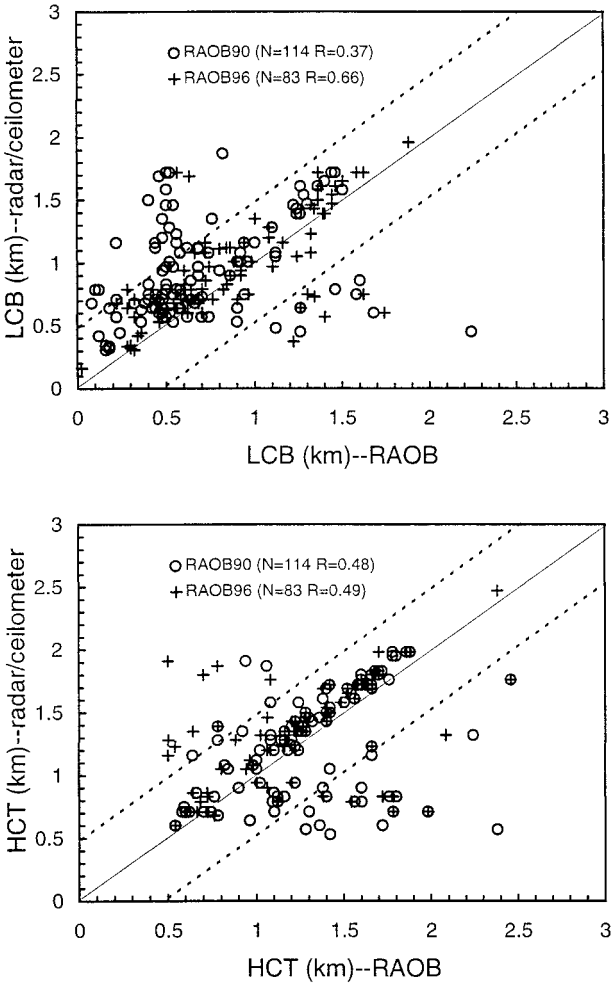

FIG. 8. Scatterplots of (upper panel) the lowest cloud-base heights AGL (LCB) and (lower panel) the highest cloud-top heights AGL (HCT) from the merged radar–ceilometer data and the rawinsonde data using the 90% alternate method (raob90) and the 96% method (raob96). The two datasets are matched in time; "N" is number of samplings, and "R" is correlation coefficient.

duces changes in the frequency distribution of cloud-top heights, as shown in Fig. 7, where randomly selecting one radar sample within half-hour bins results in a peak at 0.6–0.8 km in the cloud-top height frequency distribution, which is also shown in raob data but not in averaged radar data.

To quantify the raob results, we compare matched raob and merged radar–ceilometer observations of the base height of the lowest cloud layer (LCB) and the top height of the highest cloud layer (HCT) for all cloud layers below 3 km (Fig. 8). The 3-h raob data are matched with the 3-s merged data at the time nearest to the rawinsonde releasing time. The correlation coefficients are 0.37 and 0.48 for LCB and HCT, respectively, both of which are above 99% significance levels. The mean LCB from raob's is 679 m, 260 m lower than the radar–ceilometer value of 939 m; the mean HCT from raob's is 1376 m, only 34 m higher than the radar–ceilometer value of 1282 m. To avoid the sampling noise discussed above, we also compare raob-determined LCB and HCT with values from the merged data averaged over the half-hour time period centered at the rawinsonde release time, and three randomly sampled merged 3-s data within the half-hour time period. None of these improves the results shown in Fig. 8, implying that differences in time resolution between raob's and radar do not affect the results. We also consider the effects of horizontal drift of the rawinsonde balloon with time (average time from surface to 3 km is about 12.5 min) by comparing the raob data with the merged radar data averaged over the drifting time period. No significant improvement is made by doing this.

There are systematic underestimates of cloud base and top by about 100 m by raob's shown in Fig. 8 (points along the one-to-one line in Fig. 8). If we further increase the RH thresholds from 90% and 93% to 96% and 99%, respectively, the underestimate of cloud base is reduced by 168 m, and there are only two cases with LCB–raob at around 0.5 km but LCB from the radar data above 1 km. However, this change does not correct the systematic underestimate of cloud-top height (Fig.

8). This behavior is caused by the fact that RHs below cloud base increase gradually to saturation at cloud base, while tops are associated with sudden RH drops from saturation (see Fig. 6). Cases with higher radar-detected HCT might be explained by occasional penetration of cloud tops into the inversion base, while raob's can only locate the cloud top at the inversion base. In addition, the radar smearing problem can cause overestimate of cloud top (Miller and Albrecht 1995). We find that the average radar HCT is somewhere inside the inversion, but the raob's HCT is always at the inversion base. For cases with lower HCT from radar [differences (raob − radar) >500 m], the raob's report a double-layered cloud, but radar only detects a single-layered cloud, implying that raob's may be detecting a humid upper layer that contains no cloud. For cases with lower LCB from radar–ceilometer [differences (raob − merged) >500 m], radar reports a thin cloud layer (thinner than 120 m) below 1 km. They either correspond to small cumuli detected by radar, but missed by raob's, or are false cloud layers detected by radar because of its clutter and power leakage problems. After excluding those cases with much lower LCB and HCT in the merged data in Fig. 8 and using the 96% RH threshold for raob's, the correlation coefficients are increased to 0.85 and 0.73 from 0.37 and 0.48 for LCB and HCT, respectively.

4. Comparison of satellite-derived cloud-top locations with radar data

a. Comparison of cloud-top statistics

We compare the ISCCP cloud-top determinations in several forms for the (280 km)^2 area including Porto Santo with the raob and merged radar–ceilometer results to isolate different sources of error. The ISCCP analysis retrieves cloud-top temperature from the measured infrared radiances, but also reports the cloud-top pressure and determines the cloud-top height above mean sea level (MSL = AGL + 97 m to account for the height of the radar site) using the D1 and D2 methods (see section 2f). All ISCCP cloud-top heights discussed below are calculated by the D2 method, unless otherwise indicated. Since the ISCCP results represent an average over a rather large area compared to the point measurements of the radar, ceilometer, and rawinsonde, there may be some disagreement associated with differing spatial variations around the ground site. This effect can be exaggerated depending on whether upper-level clouds are included in the average. A particular aspect of this question is whether there is any systematic difference between the clouds over the island and the surrounding ocean because of ''island'' effects on the boundary layer.

Table 1 summarizes the average comparison between the radar–ceilometer and four ISCCP results (average over actual days of the experiment may differ slightly from full monthly mean values mentioned in section 2f): 1) ''≤3 km'' means only those pixel-level cloud-top heights that are at or below 3 km are included in the average (we use DX data for this case), 2) ''low'' means that only clouds classified as low cloud (cloud-top pressures >680 mb) from the D1 dataset are included in the average, 3) ''low + middle'' means that all clouds with top pressures >440 mb are included in the average, and 4) ''all'' means that all detected clouds are included in the average. Inclusion of all higher-level clouds changes the average cloud-top height and its standard deviation dramatically: when all clouds (only a 25% increase over low cloud amount) are included in the VIS/IR analysis, for example, the mean height increases by 600 m and the standard deviation more than doubles to >1000 m. In all the results we consider the heights obtained using both radiative transfer models: 1) ''IR'' means that the cloud-top temperature is determined assuming that the cloud emits like a blackbody and 2) ''VIS/IR'' corrects the IR emission for scattering and transmission by the clouds. The VIS/IR results are considered to be most accurate, but their average may be biased by incomplete coverage of the diurnal cycle. Thus, the ''VIS/IR ≤ 3 km'' results from the ISCCP DX dataset should be and are the best match to the radar–ceilometer statistics because of the gap in cloud occurrence from 3 to 4 km, but the ''low cloud'' results from the ISCCP D1 dataset are also a good approximation (average difference <100 m).

TABLE 1. Comparison of satellite-retrieved cloud-top heights with that from radar over Porto Santo during ASTEX in June 1992. Satellite results are averaged over an area (280 km)^2 surrounding the radar site; all results are obtained from the ISCCP D1 dataset using cloud-type information, except the ≤3 km results, which are obtained from the ISCCP DX dataset. The mean radar cloud-top height is 1370 m above mean sea level; the mean temperature and pressure at this height are 283.1 K and 870.2 mb. Average values determined by first calculating daily averages, followed by averages over date.

	VIS/IR analysis			IR analysis		
Heights included	Height (m)	Temp (K)	Pressure (mb)	Height (m)	Temp (K)	Pressure (mb)
≤3 km	1370	281.6	799	1225	282.9	815
Low	1313	282.0	803	1237	282.5	813
Low + middle	1523	280.7	776	1373	281.6	795
All	1898	278.2	755	1464	281.0	791

The ISCCP ''VIS/IR ≤ 3 km'' cloud-top heights, averaged over the (280 km)^2 area around Porto Santo for all of June 1992, happen to have the same average value as the radar cloud-top heights. Based on the amplitude and phase of the diurnal cycle of IR cloud-top heights (which agree well with the radar results, see next section), the VIS/IR average value is biased low by about 50–100 m because of incomplete diurnal coverage. The correlation of the time records of the daily mean cloud-top heights from the area-averaged satellite results (VIS/IR ≤ 3 km) and the radar is 0.48. This poorer agreement in detail can be accounted for by the

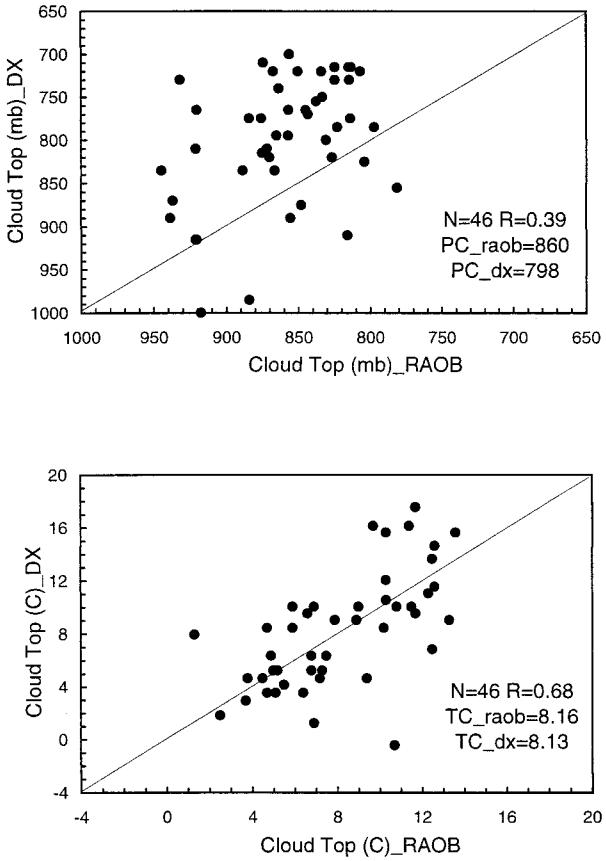

FIG. 9. Scatterplots of the lowest top pressure (mb) (PC, upper panel) and temperature (°C) (TC, lower panel) of low clouds (defined as top below 680 mb) from the ISCCP DX data of the single pixel at Porto Santo and the rawinsonde data using the 90% alternate method. The two datasets are matched in time; ''N'' is number of samplings, and ''R'' is correlation coefficient. Mean values are also given.

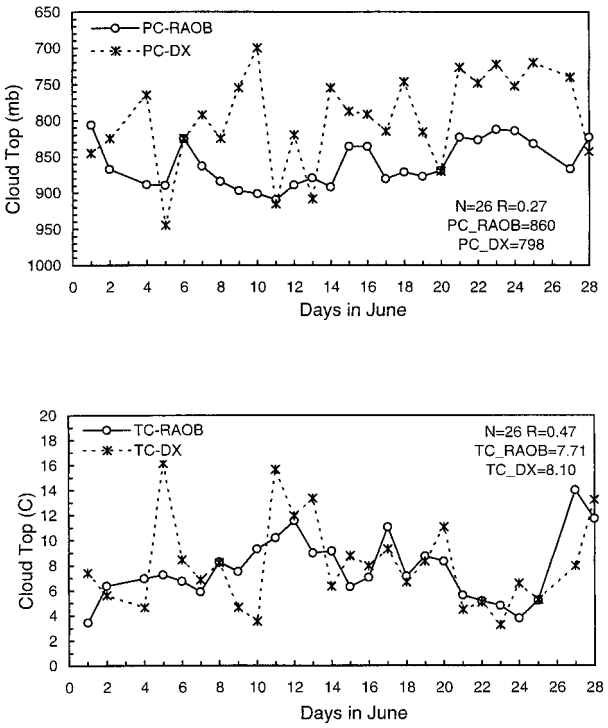

FIG. 10. Day-to-day variations of the lowest top pressure (mb) (PC, upper panel) and temperature (°C) (TC, lower panel) of low clouds (defined as top below 680 mb) from the ISCCP DX data of single pixel at Porto Santo and the rawinsonde data using the 90% alternate method; ''N'' is number of samplings, and ''R'' is correlation coefficient. Mean values are also given.

effect of comparing a pointlike measurement to an ''arealike'' measurement, if the spatial variability is large enough. Indeed, the average spatial standard deviation of satellite cloud-top heights around Porto Santo is 500 m, even when values >3 km are excluded. The temporal standard deviation of the single satellite pixel nearest Porto Santo is >600 m; thus, almost all of the time variation at one location could be accounted for simply by advection of the average spatial variability past that location. The correlation of the daily mean cloud-top heights of the single pixel at Porto Santo with the daily area mean cloud-top heights is 0.58, quantitatively similar to that obtained in comparison with the radar values. Thus, we consider the spatial sampling effect to be the main source of the ''random'' differences between the satellite and radar cloud-top heights.

To minimize the sampling problem, we compare top temperature and pressure of low clouds (PC > 680 mb) from raob's and the DX VIS/IR data for the single pixel at Porto Santo. The average cloud-top height of this one pixel is about 100 m larger than averaged over the larger area. The reason for using the raob data in this comparison, rather than the radar data, is that both report cloud-top temperature and pressure directly and have similar time sampling (every 3 h); we have shown in the previous section that the raob and radar cloud tops agree quite well. Figure 9 compares the time-matched raob and DX cloud-top pressures and temperatures (46 values). There is good agreement for cloud-top temperatures with a correlation of 0.68 and mean difference of 0.03°C. However, there is poorer agreement for cloud-top pressure: the correlation is only 0.4 and the ISCCP values are biased low by 62 mb on average. We also compared ''daily'' mean variations (where the daily average is for daytime: 0900, 1200, 1500, and 1800 UTC) in Fig. 10, showing similar results. Note that the larger differences on 5, 10, and 11 June occur because only one value was available from ISCCP on those days.

b. Explanations of disagreements

Systematic errors in the ISCCP cloud-top heights, calculated by the D2 method, will be produced by errors in the retrieved difference in the surface and cloud-top temperatures and the assumed value of the temperature lapse rate. Despite the excellent agreement with the average radar cloud-top height, the average cloud-top temperature from the ISCCP results is 1.5 K colder than

the average atmospheric temperature reported at this height by the raob's (this difference is reduced by 0.3–0.6 K accounting for the diurnal bias of the VIS/IR results). A temperature error of about 1 K is within the uncertainty of the ISCCP retrievals, associated with uncertainties in the satellite radiometer calibration, which could be as much as 1.5 K absolute (Brest et al. 1997), and with uncertainties in the radiative model treatment of water vapor absorption, which can be 0.5–1.0 K (see Rossow et al. 1989; Minnis et al. 1992). However, since the D2 method of calculating cloud-top height uses the difference between two retrieved temperatures (cloud and surface), which will minimize the systematic calibration and retrieval errors, the mismatch of cloud-top temperature and height must be produced either by errors in the assumed atmospheric properties or in the assumed atmospheric temperature lapse rate value.

Using the raob value for the temperature lapse rate, 8.3 K km^{-1}, instead of the assumed value, 6.5 K km^{-1}, reduces the ISCCP cloud-top heights by about 300 m, which is inconsistent with the underestimated cloud-top temperature. Thus, the error in the lapse rate is compensated in these results by an error in the retrieved difference in surface and cloud-top temperature. The systematic 50–70-mb low bias in the ISCCP cloud-top pressures (obtained from the operational TOVS dataset), despite excellent agreement of cloud-top temperatures with raob's, suggests that the ISCCP retrieval error may come from errors in the TOVS data. Comparison of TOVS and raob's (noted also by Minnis et al. 1992 and Stubenrauch et al. 1999) that TOVS temperatures are too large just above cloud tops by 2–3 K and that the humidity above cloud tops is also too large (cf. Randel et al. 1996). Both of these errors serve to decrease the retrieved difference in surface and cloud-top temperatures: in this particular case, these errors cause an underestimate of the temperature difference of about 2.5 K, about 20% (thus, the surface temperature is biased low relative to the cloud-top temperature), that just happens to compensate for the error in the assumed temperature lapse rate.

Table 1 illustrates another systematic error in retrieving cloud-top temperatures, common to almost all previous studies of satellite-based cloud-top temperatures for marine boundary layer clouds. These methods all assume that these low-level clouds are opaque enough to infrared radiation that they can be treated as blackbody emitters. In the ASTEX case, average visible optical thickness of the clouds from ISCCP is 5.4 for ''low'' clouds, giving an infrared optical thickness of about 2, so that their emission temperatures will appear to be slightly larger than their actual top temperatures because of radiation transmitted from below the clouds. Moreover, the observed radiation may arise from below the actual physical cloud top by as much as 20 m (Minnis et al. 1992). The average effect for all low clouds is a temperature increase of 0.5 K, height decrease of 76 m (1.3 K temperature increase, 145-m height decrease for $\leq$3 km results) (Table 1). Scattering within the cloud adds to the transmission effect slightly (a few tenths of degrees). Thus, all of these subtle effects cause an underestimate of cloud-top height based on the measured cloud-top temperature; in this case, the blackbody model yields a cloud-top height that is 145 m too low using a 6.5 K km^{-1} lapse rate (185 m for an 8.3 K km^{-1} lapse rate).

It is generally assumed that the top heights of marine boundary layer clouds can be determined accurately because they are so ''simple''; however, we have shown that there are a number of systematic effects that can cause small, but notable, biases. In particular, the common use of a blackbody assumption in determining the cloud-top temperature can bias inferred cloud-top heights low by 100–300 m because these clouds are optically thin enough to transmit some IR radiation from below. We have also illustrated the subtle effects of small errors in the atmospheric temperature and humidity just above the cloud in the inversion layer. If sufficiently accurate radiometer calibration and atmospheric temperature and humidity profiles can be obtained, cloud-top height retrieval uncertainties can be reduced to about 100 m; but, currently, the practical limit on the accuracy of marine boundary layer cloud-top heights appears to be about 150–300 m.

5. Variability of CVS

a. Vertical distribution of cloud boundaries at Porto Santo during ASTEX

The characteristics of CVS at Porto Santo during ASTEX are presented in this section using the radar–ceilometer merged data. Of 246 539 merged observations, 79% are single-layered clouds; 81% of the multilayered clouds are two layered (Fig. 4). The vertical distribution of cloud occurrence shows the predominance of clouds below 3 km (60%), a dry layer between 3 and 4 km, and the appearance of higher-level clouds over a broad range (5–11 km) of heights with a peak around 7–8 km (Fig. 3). Thus, cloud layers can be categorized as low level or upper level by whether their top or base is below or above 3 km. There are no cloud layers with a top above 3 km that have a base below 3 km. Cloud-base and -top heights have a maximum frequency of occurrence at 0.6–0.8 km and 1.2–1.4 km, respectively.

The bases of low-level, single-layered clouds have a monomodal distribution with a peak at 0.6–0.8 km, but their tops exhibit a bimodal distribution with peaks at 1.2–1.4 and 1.8–2.0 km (Fig. 11). For low-level, two-layered clouds, the tops of the uppermost layers and the bases of lowermost layers have similar distributions as single-layered clouds (Fig. 11), suggesting that these low-level, two-layered clouds might be formed from single-layered clouds when decoupling occurs (cf. Miller et al. 1998). Two-layered clouds may correspond to cumulus under stratocumulus, which was ''commonly''

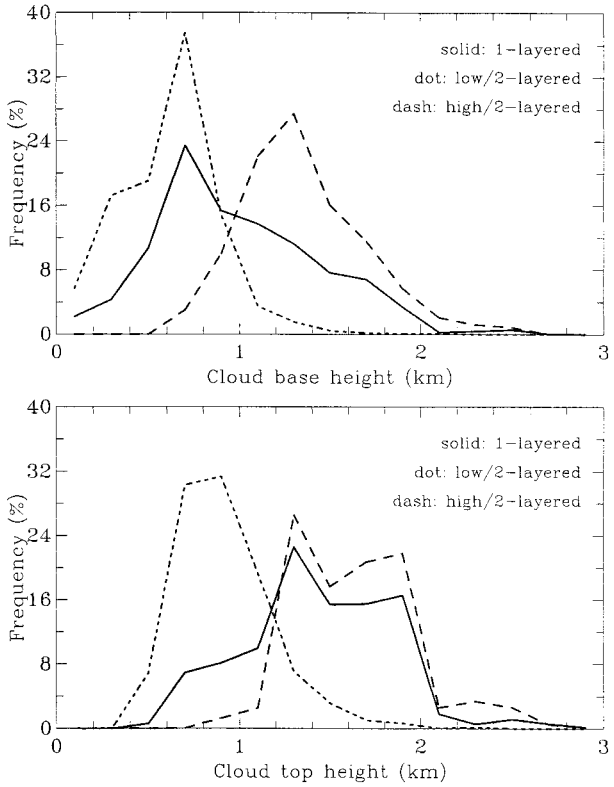

FIG. 11. Frequency distribution of (a) cloud-base and (b) -top heights AGL for single-layered and two-layered low cloud systems from the merged data.

observed during ASTEX (Albrecht et al. 1995); our data record shows that such clouds are not actually very common (see section 5c).

Cloud-layer thicknesses are <1 km 59% of the time with a mean thickness of 603 m (Fig. 3c). Low-level cloud layers that occur alone are 168 m thicker (44% of mean thickness) than those cooccurring with upper-level cloud layers both because their bases are lower (by 112 m) and because their tops are higher (by 56 m). This feature might be associated with the strong reduction of the longwave radiative cooling at the top of the lower-level cloud in the presence of the upper-layer cloud (Chen and Cotton 1987; Wang 1997). Cloud-top radiative cooling is important in recoupling the cloud and subcloud layers (Blaskoric et al. 1991; Hanson 1991), so its decrease suppresses extension of the cloud base to lower altitudes, resulting in thinner clouds. We focus on the low-level clouds below 3 km in the following.

b. Synoptic and diurnal variations of CVS at Porto Santo during ASTEX

We examine the daily and diurnal variations of the vertical structure of clouds located below 3 km from the merged radar–ceilometer data, regardless of the number of layers, in terms of the LCB, the HCT, the total cloud thickness (TCT = HCT − LCB), and the cloud amount (CA) calculated from the ceilometer data. The merged data have a time resolution of 3 s with 6-min gaps each half-hour for collecting data; the cloud amount data from the ceilometer are hourly values. In this study, we use the hourly average (of 3-s data) record in a spectral analysis to separate synoptic and diurnal variations. A minimum of 10 observations are required to calculate each hourly average. There are a total of 672 (28 × 24) hourly mean values for 28 days (1–28 June).

TABLE 2. Synoptic and diurnal variances of LCB, HCT, TCT, and CA from the merged radar–ceilometer data, the correlation coefficients of daily mean values between the merged data and raob's, and the correlation coefficients of daily mean values from the merged data among themselves.

	LCB	HCT	TCT	CA
4.5–6.8-day variance (%)	19	17.6	12.3	15
24-h variance (%)	2.8	7.1	5.2	8
Correlation coefficients with raob's	0.61	0.45	0.65	
Correlation coefficients among LCB, HCT, TCT, and CA				
LCB		0.85	−0.12	0.18
HCT			0.42	0.56
TCT				0.75

1) SPECTRAL ANALYSIS

The spectral analysis shows that the spectral densities of LCB, HCT, and TCT peak at synoptic timescales (4.5–6.8 days) and at the diurnal timescale (Table 2). However, the synoptic variability accounts for only 12%–19% of the total variance and the diurnal variations represent only 3%–8% of the total variance (Table 2); thus, most of the cloud variations during a month appear to be ''random,'' that is, occurring over all timescales within a month. However, the time record is too short to tell whether any systematic slower modes of variation are present. As suggested by Bretherton et al. (1995), the reminder of the variability is probably connected in part to the advection of the 20–100-km-wide mesoscale patches seen in satellite images of the stratocumulus clouds in the ASTEX region. This idea is supported by the ISCCP data, which show that the average spatial variability of HCT is about 35% of the mean value and nearly as large as the time variability at one location. The satellite results also show that the average diurnal range of HCT is about the same magnitude as the average horizontal variability. LCB has the largest (19%) synoptic variability, and TCT has the smallest one (12%). Meanwhile, CA has the largest (8%) diurnal variation, and LCB has the smallest (3%).

2) SYNOPTIC VARIATIONS

The merged data are averaged to obtain daily mean values. The total number of data points available for

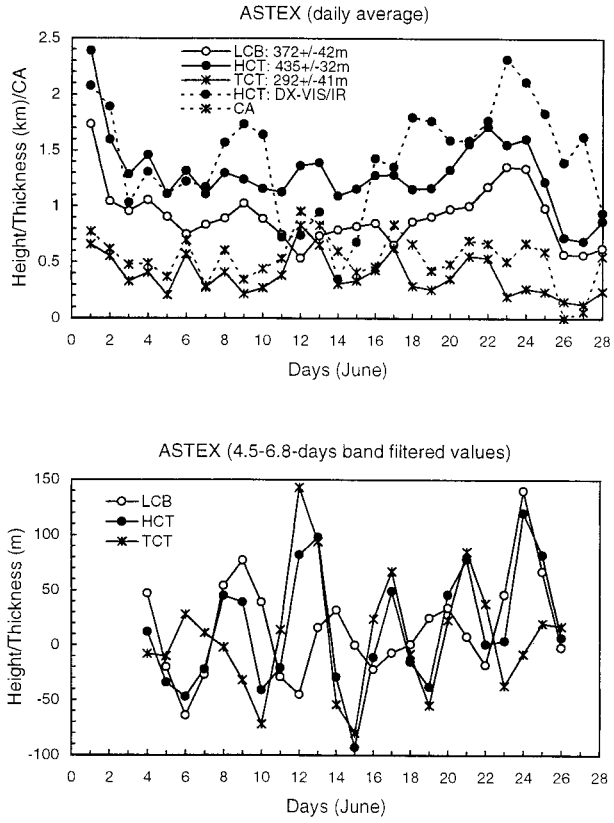

FIG. 12. Day-to-day variations of daily mean LCB, HCT, and TCT [(a), upper panel] and daily mean values after using 4.5~6.8-day band filter [(b), lower panel] from the merged data. The ranges of daily variations and errors in daily mean values are given in (a). Day-to-day variations of daily mean HCT from the ISCCP "≤3 km" VIS/IR analysis and CA are also shown in (a).

each of 28 daily mean values ranges from 12 to 24; there are at least 20 data points for 18 days out of 28 days. If no cloud is present, this number is lower. Daily mean LCB, HCT, and TCT are shown in Fig. 12a. The formal error in the daily mean values is estimated from the standard deviations of individual observations at each hour of the day divided by the square root of the number of hours used for daily mean values. The average of such estimates for 28 days is given in Fig. 12a. Daily ranges of LCB, HCT, and TCT are 9, 14, and 7 times larger than the estimated errors, respectively. The variability of cloud properties includes synoptic, diurnal, and other timescales since the sum of diurnal and synoptic variances only explains <30% of total variance (Table 2).

To minimize the contributions from other timescales, a 4.5–6.8-day band filter, which is a combination of two Lanczos filters (Duchon 1979), is applied to the time series of cloud properties (Fig. 12b). The daily variation of cloud fraction is well correlated (0.75) with daily variations of cloud-layer thickness (Fig. 12a), but the reason for this behavior has not be found. In the Tropics, cloud-top heights and the average optical thicknesses both increase as the convective complexes grow larger, which might be explained by all of these properties being determined by the magnitude of the updraft velocities in the convective towers (Machado and Rossow 1993). Some similar dynamic process may explain this correlation between cloud vertical and horizontal extensions in marine boundary layer clouds.

Daily averaged LCB, HCT, and TCT from raob's are compared with those from merged radar–ceilometer data. The synoptic variability is well captured by raob's (not shown); the correlation coefficients between the two datasets for LCB, HCT, and TCT are 0.61, 0.45, and 0.65, respectively, which are all above 95% significance levels (Table 2). The LCB from raob's is 275 m lower than that from the merged radar–ceilometer data on average. The most significant discrepancy exists when base heights are low, which may be due to overestimate of base height by the ceilometer in drizzle conditions (Albrecht et al. 1995). The satellite comparison to radar cloud-top heights shows a lower correlation of daily mean values (0.48) because of different sampling of the spatial variability (Fig. 12a). As shown in Fig. 10, the synoptic variability of cloud-top temperature is well produced by the DX data in a single pixel over Porto Santo. There may also be some systematic difference between the cloud tops at Porto Santo (over an island) and those in the whole area: the average cloud-top height in the single satellite pixel closest to Porto Santo is systematically higher than the area mean by about 100 m. The difference in temporal resolution between the merged radar (3 s) and raob–ISCCP (3 h) data can account for discrepancies in daily variations; similar differences arise between daily mean values comparing 3-s and 3-h samples of the merged data.

3) DIURNAL VARIATIONS

The diurnal variations of cloud properties are analyzed using the same method as used to study synoptic variations above. Figure 13a shows the average cloud-layer properties for each hour of the day; after using a 20–28-h filter, the diurnal cycle can be seen much more clearly (Fig. 13b). The main features of the diurnal cycle of clouds are that HCT and LCB have maxima at 0600–0800 UTC (0500–0700 LST), descending throughout the day to minima at 1600–2000 UTC. TCT exhibits a broad maximum from 0200–0600 UTC and a minimum from 1400–1800 UTC. The CA exhibits slightly more complicated changes, but generally has a maximum around 0600 UTC (0500 LST) and a minimum around 1700 UTC (1600 LST). The diurnal ranges of HCT, LCB, and TCT are much larger than the estimated errors, so these diurnal variations are significant.

The maximum HCT at 0630 UTC (0530 LST) and minimum HCT at 1630 UTC (1530 LST) measured by the radar are also well observed by the raob and the ISCCP results (see also Randall et al. 1996). The satellite-observed diurnal maximum occurs at 0600 UTC

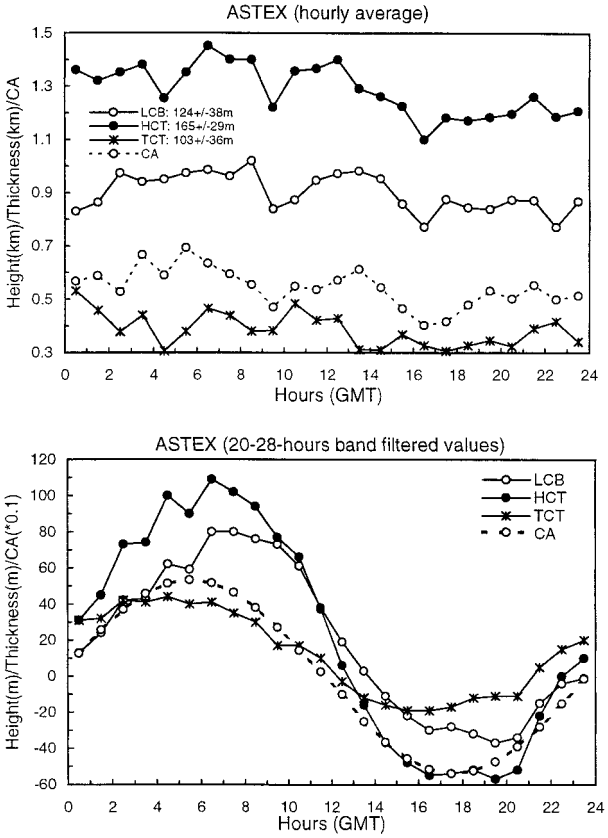

FIG. 13. Diurnal variations of hourly mean LCB, HCT, TCT, and CA [(a), upper panel] and hourly mean values after using 20~28-h band filter [(b), lower panel] from the merged data. The diurnal ranges and errors in hourly mean values are given in (a).

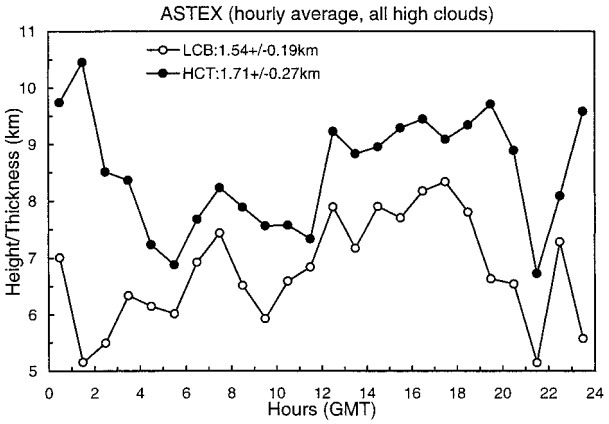

FIG. 14. Diurnal variations of hourly mean LCB and HCT for high clouds (above 3 km).

and the minimum at 1800 UTC (the ISCCP observations occur at 3-h intervals). A minimum cloud-top height occurring in the late afternoon was also found for marine stratocumulus over San Nicolas Island during FIRE87 (July 1987), but this behavior has not been fully understood (Blaskovic et al. 1991). The satellite results confirm these variations for both FIRE87 (Minnis et al. 1992) and for ASTEX (Randall et al. 1996). The phase of the diurnal cycle of cloud physical thickness resembles that of optical thickness (Cahalan et al. 1995), indicating the importance of physical thickness to determining optical thickness.

The satellite-observed diurnal amplitude of HCT is about 300 m, whereas the radar-observed amplitude is about 200 m and the raob amplitude is about 100 m. The importance of synoptic variations is illustrated in the satellite data by the fact that areawide results do not exhibit a very clear diurnal variation of HCT, if simply averaged at each time of day, but do show a clear diurnal cycle when bandpass filtered. These differences in amplitude can be accounted for by small (1.2 K) diurnal variations in temperature observed at cloud top, with a maximum in the afternoon and minimum at night, that act to exaggerate the apparent changes in cloud top as inferred from satellite temperature measurements and to diminish raob changes inferred from relative humidity measurements. Moreover, the raob data show that the cloud layers are thicker in the morning and thinner in the afternoon. Consequently, the radiation transmitted from below exaggerates the apparent diurnal cycle of cloud-top temperature. The smaller raob height change requires a slight RH increase during the day, which may be caused by decay of the cloud top by evaporation as the mixing from the surface decreases.

In section 3, we mentioned effects of high clouds on low clouds. When high clouds coexist with low clouds, low clouds do not exhibit obvious diurnal variations, suggesting an influence of high clouds on low clouds. However, this result is only tentative because there are only a few days of data from this experiment that can be used to calculate hourly mean values for this case. The higher-level clouds may also experience diurnal variations (Fig. 14): cloud layers are thickest (lower base and high top) at around local midnight (0130 UTC) and are located around 6–8 km in the morning but move up to 8–9 km in the afternoon. Such diurnal cycle variations appear to be the same whether or not low clouds are present and are out of phase with the low-level cloud diurnal cycle (see Fig. 13). The ISCCP results also show that high-level clouds exhibit a small diurnal cycle with a maximum in the afternoon. These features of the diurnal variation of high-level clouds need further study since the sample size used here is very small; high clouds occurring on 18 July (not shown) contributed most to the diurnal cycle shown in Fig. 14.

c. Characteristics of CVS in three ASTEX and the FIRE87 regions

In this section we analyze a 20-yr CVS dataset in three ASTEX and the FIRE87 regions to determinate general characteristics of CVS in those marine stratiform cloud regions. The goals are 1) to examine spatial variability of marine stratiform cloud vertical structure,

TABLE 3. Frequency (%) of occurrence of various CVS in three ASTEX and the FIRE87 regions in DJF and JJA. The frequency in each row is relative to total number of observations for that category. For example, the frequency of one-layered clouds is calculated by dividing number of one-layered low cloud observations by total number of low cloud observations. The frequency of low clouds is relative to total number of cloudy observations.

	DJF				JJA			
Description of CVS	Madeira	Azores	Ocean	FIRE87	Madeira	Azores	Ocean	FIRE87
All clouds								
One layer	75	48	65	63	87	57	75	86
Two layers	19	33	30	23	11	27	19	10
Three or more layers	6	19	6	4	2	16	6	4
Low clouds	81	86	85	78	84	92	94	98
One-layered low clouds	92	79	89	85	95	79	88	98
Two-layered low clouds	8	19	11	11	4	19	11	2
Low clouds with								
No clouds above	79	56	67	63	92	69	82	87
Only middle clouds	7	14	6	8	2	11	4	4
Only high clouds	11	21	25	20	5	14	11	7
Middle/high clouds	3	9	2	9	1	6	3	2
Two-layered low clouds								
With clouds above	38	46	44	66	9	37	33	22
With no clouds above	62	54	56	34	91	63	67	78

since as shown by the satellite results, there is significant spatial variability of cloud amount and cloud top in the area of the ASTEX experiment (see Randall et al. 1996); 2) to use the 20-yr raob dataset, instead of the 1 month of data collected during ASTEX, to determine typical CVS attributes, such as the frequency occurrence of higher clouds above low clouds. Table 3 shows the frequency of occurrence of various CVS in three ASTEX and the FIRE87 regions in December–January–February (DJF) and June–July–August (JJA).

The vertical frequency distribution of occurrence of cloudiness is displayed in Fig. 15 using 20-yr (1976–95) rawinsonde data in DJF and JJA at stations in three areas (see section 2a for details), representing three ASTEX regions (Madeira Islands, Azores Islands, and ocean). Main characteristics include the predominance of boundary layer clouds below 2 km, the relatively dry (i.e., cloud free) area between 2 and 5 km, and a broad distribution of high clouds with a peak frequency around 7–8 km (Fig. 15). In summer, more than 84% of cloudy raob's have low clouds; less than 20% of low clouds occur with any other clouds above, except over the

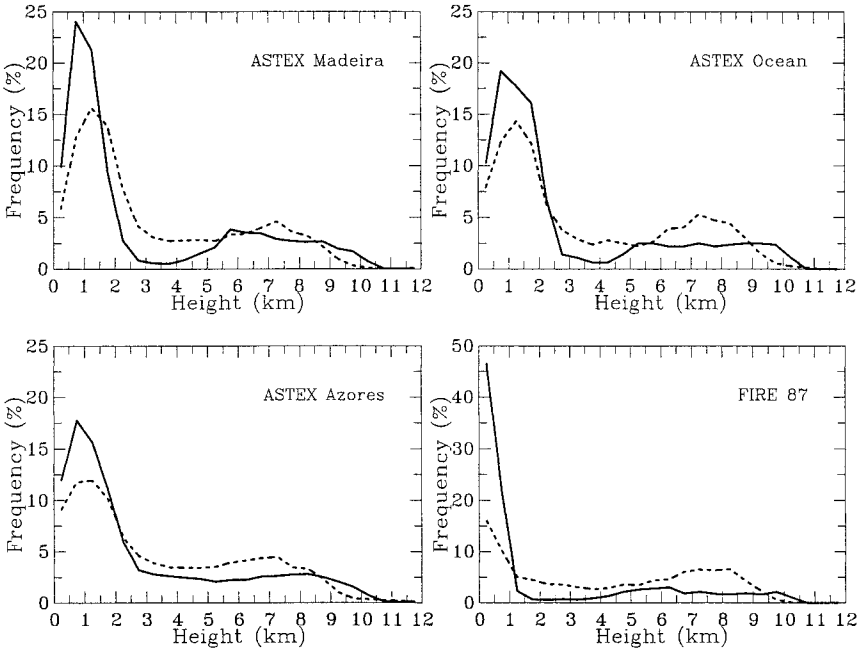

FIG. 15. Frequency distribution of cloud occurrence as a function of height MSL in three ASTEX and the FIRE87 regions in JJA (solid line) and DJF (dotted line) for all cloud layers.

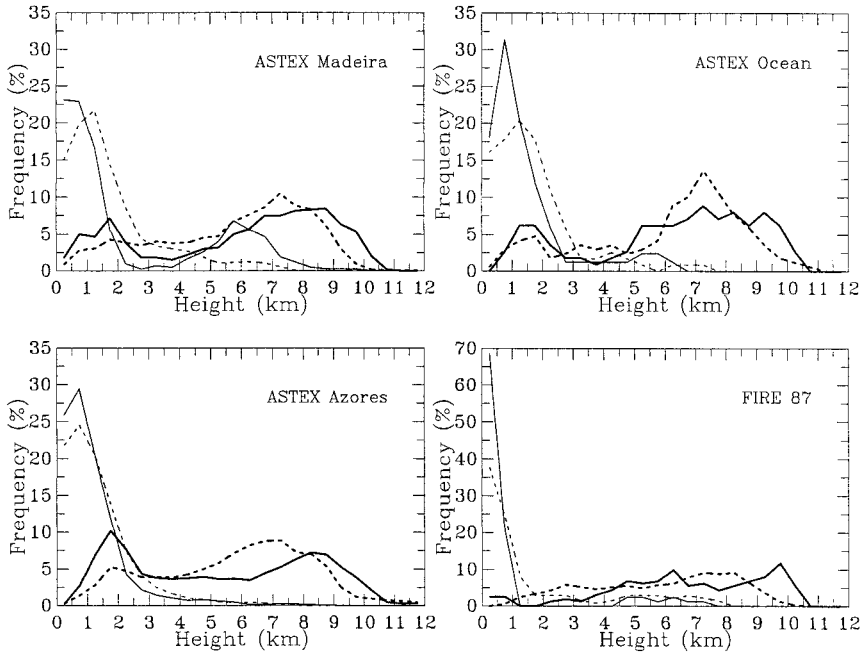

FIG. 16. Frequency distribution of cloud occurrence as a function of height MSL in three ASTEX and the FIRE87 regions in JJA (solid line) and DJF (dotted line) for two-layered cloud systems. Thick line is for higher layer; thin line for lower layer.

Azores (31%) (Table 3). These features are prominent in summer, which is why ASTEX and FIRE87 were conducted in June and July; more clouds appear above 3 km in winter than in summer (Fig. 15 and Table 3).

In summer, on average 27% of clouds are multilayered in the ASTEX regions with the highest value (43%) over the Azores Islands (Table 3). For two-layered cloud systems in the ASTEX region in summer (solid lines shown in Fig. 16), the lower layer is located primarily below 2 km, with a notable secondary peak around 5.5 km over Madeira Island, and the higher layer has a bimodal distribution peaking at near 2 and 8 km, suggesting the appearance of cumulus under stratocumulus in the boundary layer (cf. Albrecht et al. 1995) and cooccurrence of cirrus and boundary layer clouds. The frequency of double-layered low clouds (cumulus under stratocumulus) is roughly the same as that of low clouds with high clouds above (cirrus) in summer, but less in winter (Table 3). Double-layered low clouds in summer are overlaid by higher level clouds 9%, 37%, and 33% of the time in the Madeira, Azores, and ocean areas, respectively; they occur with clouds above more frequently in winter (Table 3).

In contrast to Madeira Island and the ocean regime in ASTEX, the Azores Islands, located in the northern end of ASTEX triangle area (Fig. 1), have more clouds in the dry level at 2–5 km in summer (Fig. 15) and more multilayered clouds, both double low clouds and high low clouds (Table 3). The more frequent appearance of upper-level clouds is likely due to the fact that the Azores Islands are north of Porto Santo, closer to the Atlantic storm track. Among the three regions, the Madeira Island region has the lowest frequency of multilayered clouds, both double-layered low clouds and low clouds with middle and high clouds, especially in summer (less than 10%).

FIRE87 was based on San Nicolas Island off the coast of California in June and July 1987. The analysis of cloud vertical structure shown in Figs. 15–16 and Table 3 highlights the differences between ASTEX and FIRE87. In FIRE87, marine boundary layer clouds are much lower than those in ASTEX with 46% of clouds occurring below 500 m and high clouds appearing much less frequently (Fig. 14). This is consistent with the appearance of very low-level cloud tops in the near-coastal regime in FIRE87 (Fairall et al. 1990; Minnis et al. 1992). There are also rarer occurrences of multilayered clouds (~14%), associated with extensive sheets of solid and thick (200–400 m) stratocumulus clouds in relatively shallow (600–1000 m) boundary layers (Randall et al. 1996). Unlike FIRE87, the boundary layers during ASTEX are deeper (1–2 km) and cumulus more common under the stratocumulus layer (Randall et al. 1996). Such distinctions in cloud properties in ASTEX and FIRE87 were the main motivation for the implementation of ASTEX (Albrecht et al. 1995).

The frequency distribution of cloud occurrences in data collected at Porto Santo during ASTEX agrees with that from the 20-yr raob data in JJA at two stations in

the Madeira region (Fig. 3d and Fig. 15a). The frequency of multilayered clouds for all and low clouds from the 20-yr data also corresponds to that from the radar–ceilometer data during ASTEX but is less than that from raob data during ASTEX because there were only 190 raob samples available. However, statistically significant CVS results related to the occurrence of higher level clouds shown in Table 3 can only be attained from the 20-yr raob data rather than from the limited samples in the 1 month of data collected during ASTEX. Since there are strong variations in CVS among the three ASTEX and FIRE87 regions and between DJF and JJA in each region, long-term CVS data are required to completely understand the temporal and spatial variability of marine stratiform CVS.

6. Discussion

a. The capabilities and limitations of the WR95's analysis method for marine stratiform clouds

The comparison of raob-determined cloud boundaries with radar and ceilometer observations at Porto Santo during ASTEX demonstrates that by using our analysis method raob's can detect all marine boundary layer clouds that are visible in the radar return signals and determine the top heights of all cloud layers and the base heights of cloud layers above 1 km accurately. Thus the extensive raob dataset can be an important supplement to satellite observations by providing more information about cloud-layer structure. Neglecting the presence of low clouds below cirrus can result in underestimation of cirrus cloud-top height (Baum and Wielicki 1994).

Raob's report 39% more low clouds with the base heights less than 600 m than the ceilometer and 20% more multilayered clouds than the radar for cloud layers below 3 km (Figs. 2 and 4). Global average low cloud amount is 26% (Klein and Hartmann 1993), so raob's detect approximately 10% too much low cloud globally. Average base heights of the lowest cloud layers from raob's are systematically lower than those from the radar–ceilometer merged data by about 425 m. We discovered that those disagreements are due to the fact that some of raob-detected low cloud layers might be clear moisture layers. Raising RH thresholds by 6% in our analysis method reduces the bias to about 260 m during ASTEX (Fig. 8).

b. Quantitative evaluation of ISCCP cloud tops for marine stratiform clouds

Several factors can account for the disagreements between radar and ISCCP cloud-top heights: the spatial sampling effect, biases in directly retrieved cloud-top temperature and surface temperature, errors in the assumed value of the temperature lapse rate, and errors in derived cloud-top pressure. The spatial sampling effect is a result of comparing a pointlike measurement (radar and raob's) to an arealike measurement (satellite) and is the main source of the random differences between the satellite and radar cloud-top heights. We have shown several systematic errors in retrieved cloud-top temperatures in section 4b. In particular, the common use of a blackbody assumption in determining the cloud-top temperature can bias inferred cloud-top heights low by 100–300 m. If using the D2 method to calculate cloud-top height, top-height error due to the assumption of 6.5 K km^{-1} lapse rate is about +300 m, but this was compensated by the effect of TOVS humidity and temperature errors above cloud top that produced an underestimate of the difference between the surface and cloud temperatures. The cloud-top pressures reported by ISCCP are too low by about 50–70 mb because of the warm bias of 2–3 K in the TOVS temperature profiles. If sufficiently accurate radiometer calibration and atmospheric temperature profiles can be obtained, cloud-top height retrieval errors could be reduced to about 100 m, but, currently, the practical limit on the accuracy of marine boundary layer cloud-top heights appears to be about 150–300 m. For high-level clouds cooccurring with low-level clouds during ASTEX, the satellite analyses underestimate their heights by treating them as single- rather than double-layer clouds.

c. Characteristics of CVS at Porto Santo during ASTEX

The vertical distribution of cloud occurrence shows the predominance of clouds below 3 km (60%), a dry level between 3 and 4 km, and the appearance of high clouds with a peak frequency around 7–8 km (Fig. 3). For low clouds, base and top heights have maximum frequency of occurrence at 0.6–0.8 km and 1.2–1.4 km with averages of 0.99 km and 1.41 km, respectively; layer thicknesses are less than 1 km 59% of the time with a mean of 421 m. About 90% of low clouds appear as single layers; only 10% of the cases exhibit the double-layer structure thought to indicate decoupling. About 80% of all observations have single-layered clouds; multilayered clouds are predominately two layered (81%). Two-layered clouds consist of high clouds above low clouds 48% of the time, double low clouds for 38%, and double high clouds for 14%. For double-layered low clouds, the tops of the uppermost layers and the bases of lowermost layers have similar distributions to those of single-layered clouds, suggesting that double-layered clouds are formed from single-layered clouds during decoupling events.

During ASTEX, coherent temporal variations of clouds are predominately synoptic (4.5–16.8 days) and diurnal (24 h); however, about 70%–80% of time variations at one location appear to be caused by advection of mesoscale cloud variations. On a diurnal timescale, all cloud properties (HCT, LCB, TCT, and CA) show maxima in the early morning (around 0630 UTC, 0530

LST), and minima in the late afternoon (around 1630 UTC). When high clouds coexist with low clouds, the few observations we have suggest that low clouds have no diurnal variation, while higher clouds do. Low cloud layers existing alone are 168 m thicker than those cooccurring with high cloud layers mainly because of lower base heights. The results related with high clouds, though tentative, suggest that interactions between low and high clouds require more study in the future.

d. General characteristics of CVS in three ASTEX and the FIRE87 regions

The general characteristics of CVS in three ASTEX and the FIRE87 regions are also analyzed by utilizing a 20-yr raob's dataset. All four regions are primarily covered by boundary layer clouds below 2 km, with a cloud-free layer between 2 and 5 km, and some high clouds with a peak frequency around 7–8 km (Fig. 15). The frequency of occurrence of various CVSs is shown in Table 3. There are significant amounts of multilayered clouds, particularly in winter. The CVS exhibits strong variations among the four regions and the seasons. Clearly, the 1-month dataset collected at Porto Santo during ASTEX (June 1992) is not sufficient to explore CVS seasonal variations, to sample enough high clouds to study their relation with low clouds, or to examine the occurrence of double-layered low clouds that may be associated with decoupling in the boundary layer. The more extensive raob's, supplemented by satellite observations, may be sufficient to characterize the spatial variations of CVS characteristics in other marine stratiform cloud regimes. These results illustrate the value of combinations of several datasets.

Acknowledgments. We would like to thank Drs. Roy Jenne and Abraham H. Oort for providing the global rawinsonde data. J. Wang is grateful to Dr. Judith A. Curry at the University of Colorado for support to finish writing this paper. The ceilometer and surface irradiance data were obtained from the NASA/Langley Research Center EOSDIS Distributed Active Archive Center. We thank Mathew Rothstein for assistance in processing ISCCP data. This work is supported by the NASA Global Data and Radiation Program under the direction of Dr. Robert J. Curran and National Science Foundation under Grant 962937.

REFERENCES

Albrecht, B. A., D. A. Randall, and S. Nicholls, 1988: Observations of marine stratocumulus clouds during FIRE. *Bull. Amer. Meteor. Soc.,* **69,** 618–626.

——, C. S. Bretherton, D. Johnson, W. H. Schubert, and A. S. Frisch, 1995: The Atlantic Stratocumulus Transition Experiment—ASTEX. *Bull. Amer. Meteor. Soc.,* **76,** 889–904.

AWS, 1979: The use of the skew of T, log P diagram in analysis and forecasting. AWS/TR-79/006, Air Weather Service, Scott AFB, IL, 150 pp. [Available from Air Weather Service (MAC), Scott AFB, IL 62225.]

Baum, B. A., and B. A. Wielicki, 1994: Cirrus cloud retrieval using infrared sounding data: Multilevel cloud errors. *J. Appl. Meteor.,* **33,** 107–117.

Betts, A. K., 1990: Diurnal variation of California coastal stratocumulus from two days of boundary layer soundings. *Tellus,* **42A,** 302–304.

Blaskovic, M., R. Davies, and J. B. Snider, 1991: Diurnal variation of marine stratocumulus over San Nicolas Island during July 1987. *Mon. Wea. Rev.,* **119,** 1469–1478.

Brest, C. L., W. B. Rossow, and M. D. Roiter, 1997: Update of radiance calibrations for ISCCP. *J. Atmos. Oceanic Technol.,* **14,** 1091–1109.

Bretherton, C. S., E. Klinker, A. K. Betts, and J. A. Coakley Jr., 1995: Comparison of ceilometer, satellite, and synoptic measurements of boundary-layer cloudiness and the ECMWF diagnostic cloud parameterization scheme during ASTEX. *J. Atmos. Sci.,* **52,** 2736–2751.

Cahalan, R. F., D. Silberstein, and J. B. Snider, 1995: Liquid water path and plane-parallel albedo bias during ASTEX. *J. Atmos. Sci.,* **52,** 3002–3012.

Chen, C., and W. R. Cotton, 1987: The physics of the marine stratocumulus-capped mixed layer. *J. Atmos. Sci.,* **44,** 2951–2977.

Duchon, C. E., 1979: Lanczos filtering in one and two dimensions. *J. Appl. Meteor.,* **18,** 1016–1022.

Fairall, C. W., J. E. Hare, and J. B. Snider, 1990: An eight-month sample of marine stratocumulus cloud fraction, albedo, and integrated liquid water. *J. Climate,* **3,** 847–864.

Hanson, H. P., 1991: Cloud albedo control by cloud-top entrainment. *Tellus,* **43A,** 37–48.

Intrieri, J. M., T. Uttal, W. L. Eberhard, J. B. Snider, Y. Han, J. A. Shaw, B. W. Orr, and S. Y. Matrosov, 1995: Demonstrations of multiwavelength observations and advantages for cirrus cloud studies: The FIRE II 26 November 1991 case study. *J. Atmos. Sci.,* **52,** 4079–4093.

Jin, Y., and W. B. Rossow, 1997: Detection of cirrus overlapping low-level clouds. *J. Geophys. Res.,* **102,** 1727–1737.

Klein, S. A., and D. L. Hartmann, 1993: The seasonal cycle of low stratiform clouds. *J. Climate,* **6,** 1587–1606.

Kropfli, R. A., and Coauthors, 1995: Cloud physics studies with 8 mm wavelength radar. *Atmos. Res.,* **35,** 299–314.

Machado, L. A. T., and W. B. Rossow, 1993: Structural characteristics and radiative properties of tropical cloud clusters. *Mon. Wea. Rev.,* **121,** 3234–3260.

Miller, M. A., and B. A. Albrecht, 1995: Surface-based observations of mesoscale cumulus–stratocumulus interaction during ASTEX. *J. Atmos. Sci.,* **52,** 2809–2826.

——, M. P. Jensen, and E. E. Clothiaux, 1998: Diurnal cloud and thermodynamic variations in the stratocumulus transition regime: A case study using in situ and remote sensors. *J. Atmos. Sci.,* **55,** 2294–2310.

Minnis, P., and E. F. Harrison, 1984: Diurnal variability of regional cloud and clear-sky radiative parameters derived from GOES data. Part I: Analysis method. *J. Climate Appl. Meteor.,* **23,** 993–1011.

——, D. F. Young, C. W. Fairall, and J. B. Snider, 1992: Stratocumulus cloud properties form simultaneous satellite and island-based instrumentation during FIRE. *J. Appl. Meteor.,* **31,** 317–339.

Poore, K., J. Wang, and W. B. Rossow, 1995: Cloud layer thicknesses from a combination of surface upper air observations. *J. Climate,* **8,** 550–568.

Randall, D. A., B. Albrecht, S. Cox, D. Johnson, P. Minnis, W. B. Rossow, and D. O. Starr, 1996: On FIRE at ten. *Advances in Geophysics,* Vol. 38, Academic Press, 37–177.

Randel, D. L., T. H. Vonder Haar, M. A. Ringerud, G. L. Stephens, T. J. Greenwald, and C. L. Combs, 1996: A new global water vapor dataset. *Bull. Amer. Meteor. Soc.,* **77,** 1233–1246.

Rossow, W. B., L. C. Garder, and A. A. Lacis, 1989: Global, seasonal cloud variations from satellite radiance measurements. Part I: Sensitivity of analysis. *J. Climate,* **2,** 419–458.

——, A. W. Walker, D. E. Beuschel, and M. D. Roiter, 1996: Inter-

national Satellite Cloud Climatology Project (ISCCP) documentation of new cloud datasets. WMO/TD-737, World Climate Research Programme, Geneva, Switzerland, 115 pp.

Rozendaal, M. A., C. B. Leovy, and S. A. Klein, 1995: An observational study of diurnal variations of marine stratiform cloud. *J. Climate,* **8,** 1795–1809.

Sassen, K., 1991: The polarization lidar technique for cloud research: A review and current assessment. *Bull. Amer. Meteor. Soc.*, **72,** 1848–1866.

Schubert, W. H., S. K. Cox, T. B. McKee, D. A. Randall, P. E. Ciesielski, J. D. Kleist, and E. L. Stevens, 1992: Analysis of sounding data from Porto Santo Island during ASTEX. Department of Atmospheric Science, Colorado State University, Atmospheric Science Rep. 512, 96 pp. [Available from Department of Atmospheric Science, Colorado State University, Fort Collins, CO 80523.]

Short, D. A., and J. M. Wallace, 1980: Satellite-inferred morning-to-evening cloudiness changes. *Mon. Wea. Rev.*, **108,** 145–165.

Stubenrauch, C. J., W. B. Rossow, F. Cheruy, A. Chedin, and N. A. Scott, 1999: Clouds as seen by satellite sounders (3I) and imagers (ISCCP). Part I: Evaluation of cloud parameters. *J. Climate,* **12,** 2189–2213.

Uttal, T., L. I. Church, B. E. Martner, and J. S. Gibson, 1993: CLDSTATS: A cloud boundary detection algorithm for vertically pointing radar data. NOAA Tech. Memo. ERL WPC-233, 28 pp. [Available from Taneil Uttal, NOAA/ERL/ETL, 325 Broadway, Boulder, CO 80303.]

——, E. E. Clothiaux, T. P. Ackerman, J. M. Intrieri, and W. L. Eberhard, 1995: Cloud boundary statistics during FIRE II. *J. Atmos. Sci.*, **52,** 4276–4284.

Wang, J., 1997: Determination of cloud vertical structure from upper air observations and its effects on atmospheric circulation in a GCM. Ph.D. thesis, Columbia University, 233 pp. [Available from Junhong Wang, NCAR/SSSF, P. O. Box 3000, Boulder, CO 80307-3000.]

——, and W. B. Rossow, 1995: Determination of cloud vertical structure from upper-air observations. *J. Appl. Meteor.*, **34,** 2243–2258.